Check for updates

Received: 28 December 2023 | Revised: 9 April 2024 | Accepted: 11 April 2024

DOI: 10.1002/bkcs.12845

PERSONAL ACCOUNT

BKCS BULLETIN OF THE KOREAN CHEMICAL SOCIETY

Gold nanoshells with varying morphologies through templated surfactant-assisted seed-growth method

Sunghee Lee | **Soyun Lee** | **Soojin Hwang** | **So-Jung Park**

Department of Chemistry and Nanoscience, Ewha Womans University, Seoul, Korea

Correspondence
So-Jung Park, Department of Chemistry and Nanoscience, Ewha Womans University, Seoul 03760, Korea.
Email: sojungpark@ewha.ac.kr

Abstract

Plasmonic nanoparticles exhibit dramatic changes in optical properties depending on their spatial organization. Therefore, the ability to precisely control their assembly structure is important for both fundamental understanding and practical applications. In this personal account, we describe a templated surfactant-assisted seed-growth method to synthesize core–shell-type gold nanoparticle assemblies with controllable surface morphologies and optical properties. This approach provides a simple procedure for simultaneous growth and assembly of metal nanoparticles on polymer templates, producing well-defined nanostructures such as spiky nanoshells and raspberry-like metamolecules with useful and interesting optical properties, such as strong and uniform surface-enhanced Raman scattering and metamaterial properties. We discuss the factors that control the morphology and collective properties, describe the design rules acquired from the system, and suggest future directions of this research area.

KEYWORDS
metal nanoshell, optical magnetism, plasmonic, SERS, synthesis

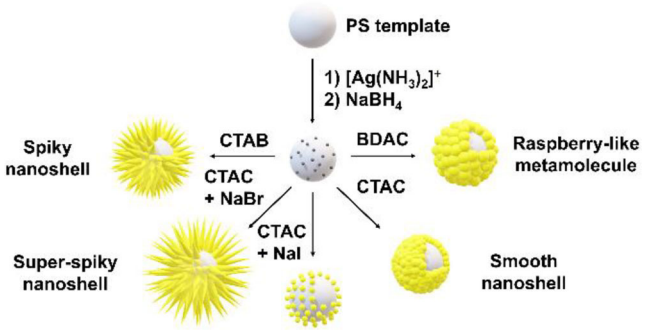
INTRODUCTION

Plasmonic metal nanoparticles have received great attention, owing to their unique optical properties that originate from the localized surface plasmon resonance (LSPR).[1–3] The LSPR position and strength can be tuned by varying the size, shape, and composition of nanoparticles, as well as the surrounding dielectric environment.[4–6] Furthermore, new properties emerge when nanoparticles are organized with less than a few nanometer separations.[7,8] Such collective properties include distance-dependent spectral shifts,[9–11] near-field enhancement,[12–14] chirality,[15,16] and optical magnetism.[17–20] As such, plasmon coupling between nanoparticles provides a powerful strategy to achieve highly tunable optical properties useful for various applications.[21–24]

Fabrication methods for plasmonic nanoparticle assemblies can be divided into top-down lithographic techniques[25–30] and bottom-up chemical approaches.[31–41] Top-down techniques such as electron beam lithography allow for precise fabrication of the desired assembly structures. However, they are mostly limited to two-dimensional structures and can produce only a small number of assemblies at a time. Therefore, significant efforts have been devoted to developing bottom-up chemical approaches based on solution-phase synthesis and self-assembly, which enable the scalable production of plasmonic assemblies at low costs. A common approach relies on the self-assembly of pre-synthesized nanoparticles through chemical and biological interactions (e.g., electrostatic,[31,37,38,41–43] metal-ligand,[31,39,44] and biomolecular[34,36] interactions). Another approach is based on the

Dedicated to Professor Sung-Jin Kim's achievements and contributions to scientific societies in Korea.

This is an open access article under the terms of the Creative Commons Attribution-NonCommercial-NoDerivs License, which permits use and distribution in any medium, provided the original work is properly cited, the use is non-commercial and no modifications or adaptations are made.
© 2024 The Authors. *Bulletin of the Korean Chemical Society* published by Korean Chemical Society and Wiley-VCH GmbH.



SCHEME 1 Schematic description of templated surfactant-assisted seed-growth method. Reproduced with permission.[21] Copyright 2021, Wiley-VCH.

templated synthesis of metal nanoparticles, where the growth of metal nanoparticles on a template leads to in situ assembly formation. Recent developments in these bottom-up synthetic and self-assembly methods have significantly improved our understanding of the collective properties of plasmonic nanoparticles.[21,45]

In this personal account, we discuss a templated surfactant-assisted seed-growth method to synthesize gold nanoparticle assemblies with tunable surface morphologies and optical properties (Scheme 1).[35,46–48] This approach enables the simultaneous one-step synthesis and assembly of metal nanoparticles with different morphologies, such as smooth, spiky,[46,47,49] and super-spiky[48] nanoshells, as well as raspberry-like metamolecules (raspberry-MMs)[35,50–52]; these systems show interesting optical properties, such as tunable surface plasmon resonance (SPR),[48] reliable surface-enhanced Raman scattering (SERS),[47,49,50,52] and optical magnetism.[35,51] We conclude the account with a discussion of current challenges and future directions in this research area.

GENERAL SYNTHETIC APPROACH

The templated surfactant-assisted seed-growth method combines the surfactant-assisted seed-mediated metal growth and the templated synthesis of nanoparticles to generate spherically arranged metal nanoparticles (Scheme 1).[35,46–48] Typically, small silver particles are first synthesized using a strong reducing agent, such as sodium borohydride, on negatively charged carboxylate-modified polystyrene (PS) beads. The electrostatic interaction between the positively charged silver complexes and the negatively charged PS beads results in uniformly distributed silver seed particles on the surface of PS beads. These seed-decorated PS templates are subsequently added to a growth solution containing $HAuCl_4$, $AgNO_3$, ascorbic acid, and cationic surfactants, which leads to the growth of gold nanoparticles from the silver seeds on the PS templates. The shape of the particles can be controlled by varying the surfactants and other additives (e.g., metal ions, halides) in the growth solution, as illustrated in Scheme 1.[35,48]

SPIKY NANOSHELLS

The combination of cetyltrimethylammonium bromide (CTAB) and silver nitrate additives in the growth solution generates closely packed spiky gold nanoparticles on PS cores, denoted as spiky gold nanoshells (Figure 1a, blue).[46,47] Silver ions are necessary for the formation of uniform spiky shell structures (Figure 1b). Without silver ions, a rapid reduction of gold occurs, which leads to the formation of large polydisperse gold nanoparticles on the PS core.[47] Replacing CTAB with cetyltrimethylammonium chloride (CTAC) results in the formation of quasi-spherical nanoparticles fused into a smoother shell structure, denoted as smooth nanoshell (Figure 1a, red).[48] This behavior is consistent with the results of homogeneous seed-mediated growth methods, in which the use of CTAC and CTAB surfactants yields nanospheres[53,54] and nanorods,[55,56] respectively. The growth of anisotropic, rod-shaped particles with CTAB has been attributed to the facet-selective binding of bromide ions on growing nanoparticles.[57]

The shape of the nanoparticles can be controlled by introducing additional halide ions in the growth solution. The combination of CTAC and bromide ions can generate super-spiky nanoshells with much sharper and denser one-dimensional (1D) nanoparticles, in which the seed-decorated PS core/gold precursor ratio as well as the bromide concentration determines the sharpness and density of the spikes (Figure 1a, green and magenta).[48] The combination of CTAC and bromide ions provides a better control over the nanoparticle growth than the CTAB growth solution, as the concentration of surfactants and halides can be adjusted separately to obtain optimal condition for controlling the shape of nanoparticles. The CTAC/iodide combination produces incomplete shell structures with quasi-spherical nanoparticles, due to the strong binding of iodide ions to growing gold particles.[48] These observations indicate that the shape-control mechanism found in the homogeneous surfactant-assisted seed growth method is generally applicable to the templated synthesis of nanoparticles with different morphologies.

The surface morphology significantly affects optical properties of gold nanoshells.[58,59] For typical smooth nanoshells, the SPR position can be controlled by varying the shell thickness relative to the overall size, and they show red-shifts into the near IR region with decreasing shell thickness.[60,61] In contrast, the SPR position of spiky nanoshells showed a red-shift over a broad range of wavelengths with increasing spike length (Figure 1c, top),[48] consistent with the simulated spectra (Figure 1c, bottom). Experimental data are broader than simulated ones as experimental spectra represent ensemble-averaged data over many individual nanoshells with structural

12255949, 2024, 6, Downloaded from https://onlinelibrary.wiley.com/doi/10.1002/bkcs.12845 by Ewha Womans University Library, Wiley Online Library on [16/01/2025]. See the Terms and Conditions (https://onlinelibrary.wiley.com/terms-and-conditions) on Wiley Online Library for rules of use; OA articles are governed by the applicable Creative Commons License

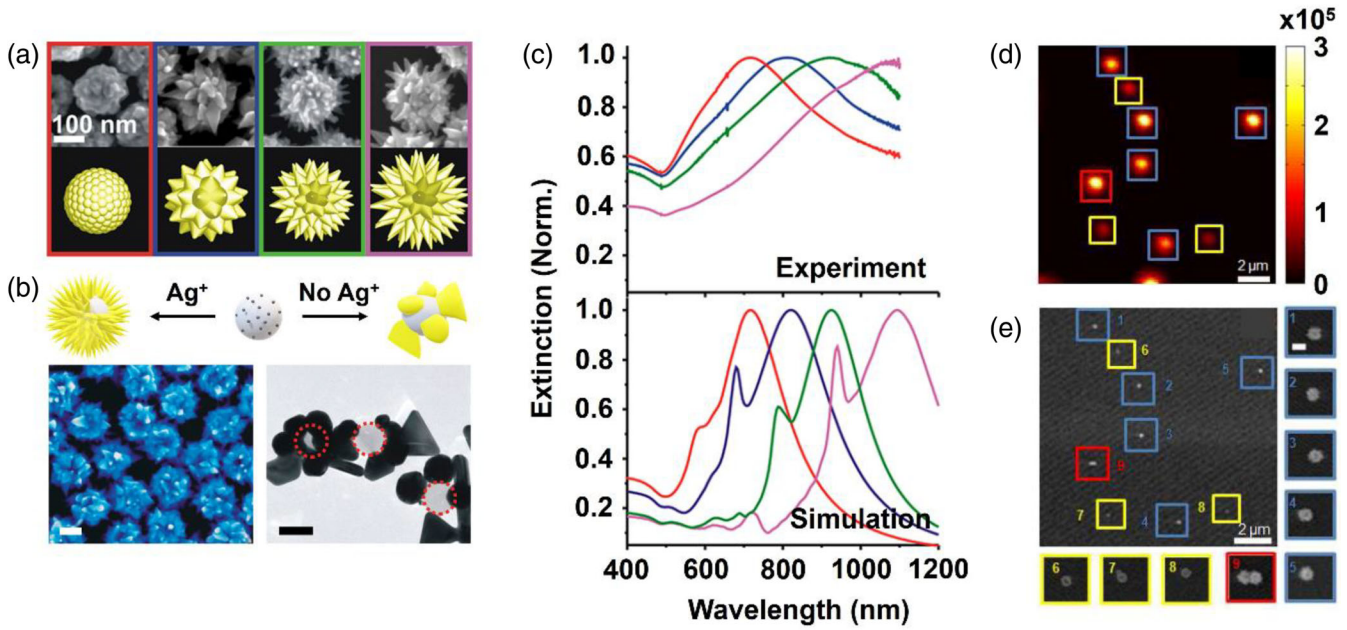


FIGURE 1 Smooth and spiky nanoshells with controllable SPR properties. (a) SEM images and simulated models of smooth (red), spiky (blue), and super-spiky (green and magenta) nanoshells. (b) Electron microscope images of nanoshells obtained with or without $AgNO_3$ in the growth solution. The PS cores are highlighted with dotted red lines in the TEM image on the right. Scale bar: 200 nm. (c) Experimental and simulated extinction spectra of smooth, spiky, and super-spiky nanoshells, as shown in a. Each spectrum displayed in c corresponds to the gold nanoshells highlighted in (a). (d, e) Dark-field scattering (d) and corresponding SEM (e) images of spiky (blue boxes) and smooth (yellow boxes) nanoshells. (a, c) Reproduced with permission.[48] Copyright 2013, American Chemical Society. (b, d, e) Reproduced with permission.[47] Copyright 2012, American Chemical Society.

heterogeneity. Figure 1d, e presents the single-particle far-field scattering and corresponding scanning electron microscopy (SEM) images of smooth and spiky nanoshells spread on a single substrate, highlighting a stronger far-field scattering from spiky nanoshells.[47] These results provide a design guideline for nanoparticles with enhanced scattering properties in the near-infrared region.

Spiky nanoshells composed of densely packed 1D particles with sharp ends exhibit strong local electric fields at the tips and valleys, as revealed by finite-difference time-domain (FDTD) simulations (Figure 2a).[47] These structural characteristics suggest that spiky nanoshells are excellent SERS platforms, as they contain abundant hot spots at the sharp tips and interparticle junctions. In fact, single-particle SERS measurements show intense SERS signals from 4-mercaptobenzoic acid (4-MBA) immobilized on spiky nanoshells (Figure 2b).[47] The smooth nanoshells with immobilized 4-MBA do not produce detectable SERS signals at the single-particle level, although they show intense signals as particle dimers and clusters. In contrast, spiky nanoshells possess numerous built-in hot spots, producing highly reproducible and strong SERS signals at the single-particle level.

The SERS data obtained for spiky nanoshells show an interesting wavelength dependence. Figure 3a presents the single-particle SERS intensities of 4-MBA immobilized on spiky nanoshells obtained with two different excitation wavelengths (633 nm, 785 nm), which showed that 633 nm excitation generated an approximately 20 times stronger SERS signal with a narrower intensity distribution compared to 785 nm excitation (Figure 3a).[49] FDTD simulations for ordered and disordered structures revealed that the wavelength dependence is due to the heterogeneity of the spiky nanoshell structure (e.g., spike length) and that the dark quadrupole mode plays an important role for the Raman enhancement. Disordered nanoshells with varying spike lengths can support additional quadrupole modes that are absent in ordered spiky nanoshells with identical spikes or in smooth nanoshells. The additional quadrupole modes contribute significantly to the SERS enhancement, which explains the strong SERS signal observed for the disordered spiky nanoshell as well as the wavelength dependence in its SERS enhancement factor (Figure 3b). It is interesting to note that the introduction of disorder significantly increases the SERS enhancement (Figure 3b).[49] Moreover, the SERS signal distribution is narrower for the quadrupole excitation at 633 nm (Figure 3a), which is attributed to the broad quadrupole mode of disordered spiky nanoshells. These results indicate that some degree of heterogeneity can lead to stronger and more reproducible SERS signals, providing an important design rule for SERS substrates.

RASPBERRY-LIKE METAMOLECULES

As described above, the surface morphology of gold nanoshells can be readily controlled by varying the

12255949, 2024, 6, Downloaded from https://onlinelibrary.wiley.com/doi/10.1002/bkcs.12845 by Ewha Womans University Library, Wiley Online Library on [16/01/2025]. See the Terms and Conditions (https://onlinelibrary.wiley.com/terms-and-conditions) on Wiley Online Library for rules of use; OA articles are governed by the applicable Creative Commons License

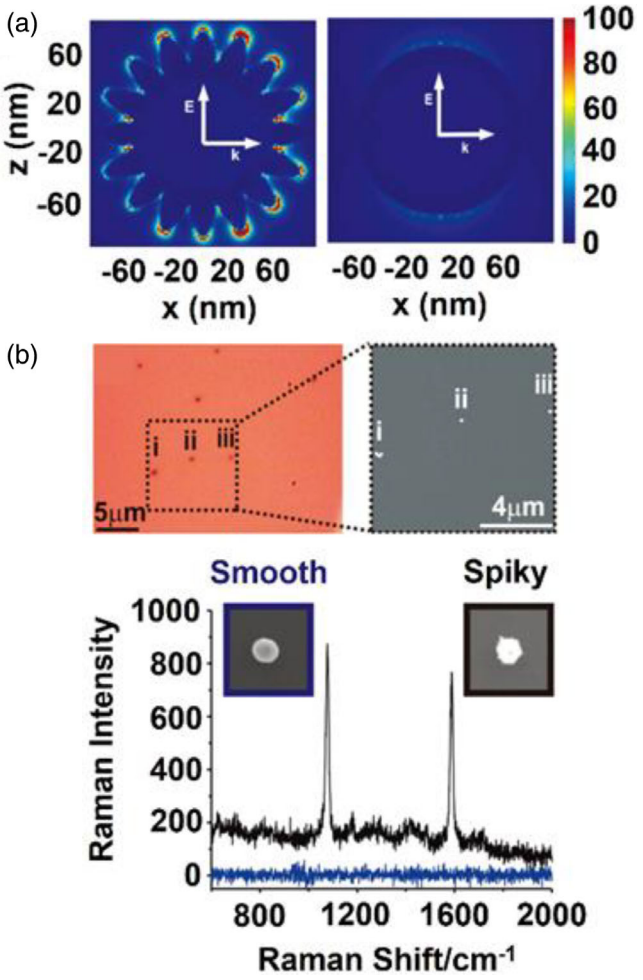


FIGURE 2 (a) Electric field maps of smooth (right) and spiky (left) nanoshells. (b) Single-particle SERS spectra of 4-MBA immobilized on smooth (blue) and spiky (black) nanoshells. Optical and SEM images of spiky nanoshells used for SERS measurements are given on top. Reproduced with permission.[47] Copyright 2012, American Chemical Society.

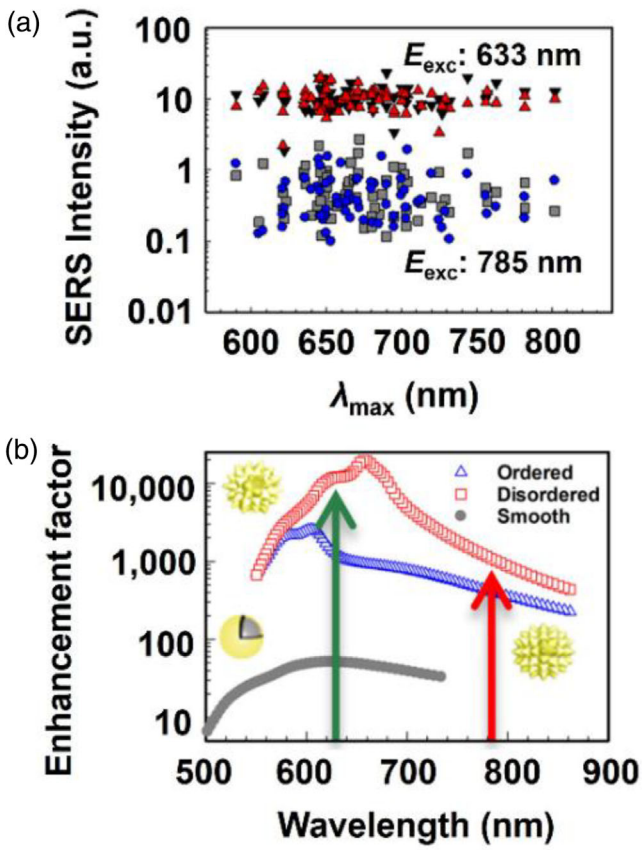


FIGURE 3 Single-particle SERS collected from spiky nanoshells with two different excitation wavelengths. (a) SERS intensities at 1077 cm^{-1} (black triangle, gray square) and 1585 cm^{-1} (red triangle, blue circle) Stokes scattering collected with 633 nm and 785 nm excitation plotted against the dark field scattering peak position (λ_{max}). (b) Calculated Raman enhancement factor of 1077 cm^{-1} Stokes scattering line for ordered spiky (blue), disordered spiky (red), and smooth (gray) nanoshells. Green and red arrows show the extinction excitation wavelengths used for Raman scattering. Reproduced with permission.[49] Copyright 2014, American Chemical Society.

type of cationic surfactants and ionic additives in the growth solution. Benzyldimethylhexadecylammonium chloride (BDAC), an aromatic surfactant, produces raspberry-like nanoshells (Figure 4a, b), denoted as raspberry-like metamolecules (raspberry-MMs) for its optical magnetism (vide infra).[35] The use of a BDAC-based growth solution leads to the generation of BDAC-coated spherical gold nanoparticles on PS cores, resulting in densely packed nanosphere assemblies without physical contact. The discrete nature of the nanospheres composing raspberry-MMs was confirmed by replacing BDAC with thiolated polyethylene glycol (PEG) (Figure 4a). The dispersion of PEG-modified raspberry-MMs in ethanol caused swelling of PEG, loosening the close packing of nanospheres on PS templates (Figure 4c). The loosely bonded nanospheres could be further broken apart into individual nanospheres by sonication (Figure 4d). The extinction spectra were consistent with the electron microscopy observations (Figure 4e). The raspberry-MMs exhibit an unusually broad extinction spectrum covering the visible and NIR regions (Figure 4e, green). After the PEG modification and ethanol dispersion, the spectrum shows a drastic blue shift (Figure 4e, black), resembling that of isolated nanoparticles. Upon sonication, the extinction in the NIR region is further reduced (Figure 4e, red), confirming that the nanospheres making up raspberry-MMs are not in physical contact. The discrete nature of gold nanospheres in raspberry-MMs was attributed to the tight packing of the aromatic surfactant, BDAC, on nanospheres, which prevents them from fusing together. Taken together, the synthetic procedure generates spherical nanoparticles densely packed on PS cores separated by a thin BDAC layer.

Plasmonic nanoparticles forming a loop structure can support magnetic resonances at optical frequencies through the displacement current.[17–19] Small interparticle gaps in the loop can sustain circulation of the localized electric field, inducing the interaction with the magnetic

12255949, 2024, 6, Downloaded from https://onlinelibrary.wiley.com/doi/10.1002/bkcs.12845 by Ewha Womans University Library, Wiley Online Library on [16/01/2025]. See the Terms and Conditions (https://onlinelibrary.wiley.com/terms-and-conditions) on Wiley Online Library for rules of use; OA articles are governed by the applicable Creative Commons License

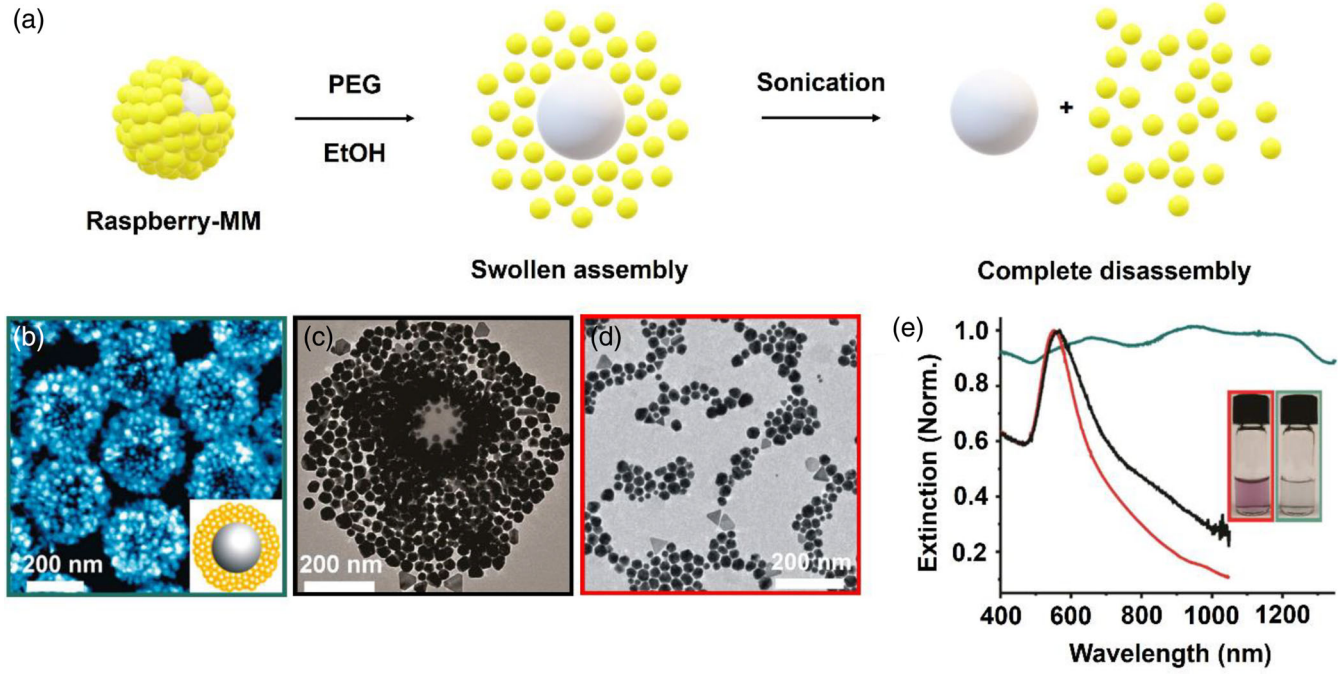


FIGURE 4 (a) Schematic description of the disassembly process used to confirm the discrete nature of gold nanospheres on a PS core. (b) SEM image of raspberry-MMs. (c) TEM image of PEG-modified raspberry-MM dispersed in ethanol. (d) TEM image of isolated gold nanospheres after sonication. (e) Extinction spectra of raspberry-MMs (b, green), swollen assembly (c, black), and completely disassembled nanoparticles (d, red). The inset show photographs of the raspberry-MM solution shown in b and the isolated gold nanoparticle solution after sonication shown in d. (a) Reproduced with permission.[21] Copyright 2021, Wiley-VCH. (b–e) Reproduced with permission.[35] Copyright 2015, American Chemical Society.

field of incident light normal to the plane of the nanoparticle loop. As such, raspberry-MMs composed of densely packed gold nanospheres can interact with the magnetic field of the incident light, resulting in strong magnetic resonances (Figure 5).[35] The calculated extinction cross-sections and mode analyses show that the magnetic dipole resonance contributes significantly to the extinction spectrum at longer wavelengths (Figure 5a, b). The emergence of strong magnetic resonances was experimentally confirmed by polarization-dependent far-field scattering measurements (Figure 5c), in which the electric and magnetic dipole scattering spectra of raspberry-MMs were separately collected using different polarization settings of the incident and scattered light. The data reveal an unusually strong magnetic dipole in the NIR region, with intensity comparable to that of the electric dipole resonance. Similar core–shell-type nanoparticle assemblies have been fabricated by the self-assembly of pre-synthesized nanoparticles on polymer or silica cores through various chemical and biological interactions.[31–34,37,39] However, in general, it is difficult to achieve the high nanoparticle density necessary for strong magnetic resonances through self-assembly routes. Another challenge is to maintain short interparticle distances without physical fusion. In raspberry-MMs,[35] gold nanoparticles are well-protected by the aromatic BDAC surfactants, which separate them by an average distance of approximately 2 nm. The closely packed assembly structure is responsible for the strong magnetic resonance observed in raspberry-MMs. It is also worth noting that the magnetic resonance is observed regardless of the polarization direction in the isotropic three-dimensional assembly structure of raspberry-MMs.

Systematic computational studies were carried out to investigate how the electric and magnetic dipole resonances respond to changes in various structural parameters, such as interparticle distance and nanoparticle size (Figure 6a).[51] For both electric and magnetic dipole resonances, the wavelength and strength increase with decreasing interparticle distance (Figure 6b, c) and increasing nanoparticle size (Figure 6d, e). However, the magnetic resonance strength shows a greater dependence on the interparticle distance than the electric resonance. The localized electric field in the interparticle gap modulates the strength of the rotating polarization currents that generate magnetic resonances normal to the nanoparticle loop. As such, the magnetic resonance is more sensitive to the interparticle distance and optical coupling than the electric resonance. The interparticle distance dependence was experimentally confirmed by using aromatic surfactants with different alkyl lengths in the synthesis of raspberry-MMs.[51] The results provide guidelines for designing plasmonic metamolecules with the desired magnetic resonant wavelength and strength.

Like spiky nanoshells, raspberry-MMs show bright and highly reproducible SERS signals at the single-particle level, because they contain numerous built-in hot spots in

12295949, 2024, 6, Downloaded from https://onlinelibrary.wiley.com/doi/10.1002/bkcs.12845 by Ewha Womans University Library, Wiley Online Library on [16/01/2025]. See the Terms and Conditions (https://onlinelibrary.wiley.com/terms-and-conditions) on Wiley Online Library for rules of use; OA articles are governed by the applicable Creative Commons License

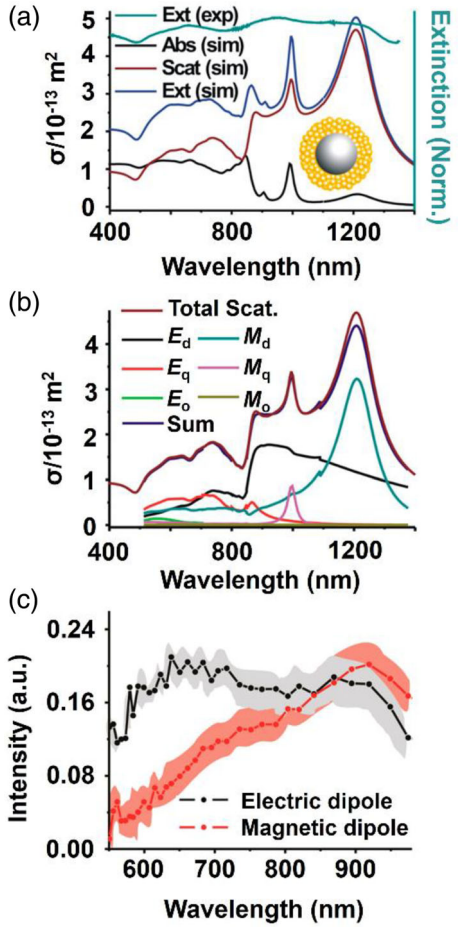


FIGURE 5 (a) Experimental extinction spectrum of raspberry-MMs along with simulated absorption and scattering cross-sections of a raspberry-MM model. (b) Simulated scattering cross-sections of different electric and magnetic modes (E_d: electric dipole, E_q: electric quadrupole, E_o: electric octupole, M_d: magnetic dipole, M_q: magnetic quadrupole, M_o: magnetic octupole) and sum of the cross-sections of all six calculated electric and magnetic modes. The total scattering spectrum obtained by FDTD simulations is included for comparison. (c) Measured electric and magnetic dipole intensity of a raspberry-MM. Reproduced with permission.[35] Copyright 2015, American Chemical Society.

interparticle gaps.[50,52] The degree of Raman enhancement was dependent on the structural parameters of raspberry-MMs such as the overall size of raspberry-MMs as well as the size of gold nanoparticles.[50] A bimodal imaging method that simultaneously measures SERS and Mie scattering signals (Figure 7a) was employed to correlate two signals from the same spots for raspberry-MMs and nanocubes immobilized with 4-MBA (Figure 7b, c).[52] The bright spots in the Mie scattering images indicate the location of nanoparticles. Therefore, the comparison between the SERS and Mie scattering images provides the population of SERS-active and SERS-inactive spots. In the case of nanocubes, many bright spots in the Mie scattering images are SERS-inactive because a strong SERS activity requires the formation of small gaps between nanoparticles (Figure 7b). In contrast, most raspberry-MMs show both SERS and Mie scattering signals, indicating that they are SERS-active as isolated single particles, without the need to form nanoparticle junctions (Figure 7c). Furthermore, the SERS signal from raspberry-MMs shows a weak dependence on the cluster number and interparticle distance (Figure 7d, e).[50] In general, the SERS signal is highly dependent on the distance between nanoparticles (Figure 7e, triangle and circle).[62,63] In contrast, raspberry-MM dimers with different interparticle distances show a narrow intensity distribution, revealing distance-independent SERS (Figure 7e, square). This unique property is attributed to the large number of built-in hot spots in individual raspberry-MM particles. Although the dimerization creates a new hot spot, it does not contribute significantly to the overall SERS intensity. This property is useful for SERS-based sensing, as it reduces spurious signals due to the aggregation of nanoparticles.

SUMMARY AND PERSPECTIVE

In this paper, we reviewed a synthetic approach to the controlled assembly of nanoparticles.[35,46–52] The approach combining the templated metal growth and seed-mediated nanoparticle synthesis provides a simple one-step procedure for the simultaneous synthesis and assembly of metal nanoparticles. The metal growth on a polymer core decorated with small seed nanoparticles generates metal nanoparticles with various shapes and sizes on the polymer core. The type of surfactant in the growth solution plays an important role in controlling the morphology. The introduction of CTAC, CTAB, and BDAC in the growth solution generates smooth nanoshells with a rough surface,[48] spiky nanoshells,[46–49] and raspberry-MMs,[35,50–52] respectively. Smooth nanoshells are composed of gold nanoparticles fused together into a continuous shell on dielectric beads. Spiky nanoshells are composed of sharp 1D spikes radially arranged on dielectric beads. Raspberry-MMs are composed of quasi-spherical nanoparticles closely packed on dielectric beads. An important goal in this research area is to develop a straightforward low-cost method for synthesizing large quantities of plasmonic nanoparticle assemblies with the desired functionalities. The approach reviewed here provides a simple methodology for synthesizing well-defined nanoparticle assemblies with desired architectures and does not involve expensive chemicals or multistep procedures.

The nanoparticle assemblies exhibit interesting optical properties. Spiky nanoshells showed red-shifted spectra from that of smooth nanoshells with the wavelength increasing with the length of spikes. Spiky nanoshells show significantly enhanced far-field and near-field scattering compared to smooth nanoshells and serve as excellent SERS substrates at the single-particle level. The raspberry-MMs show unusually strong magnetic resonances and broad extinction spectra, owing to the closely

12255949, 2024, 6, Downloaded from https://onlinelibrary.wiley.com/doi/10.1002/bkcs.12845 by Ewha Womans University Library, Wiley Online Library on [16/01/2025]. See the Terms and Conditions (https://onlinelibrary.wiley.com/terms-and-conditions) on Wiley Online Library for rules of use; OA articles are governed by the applicable Creative Commons License

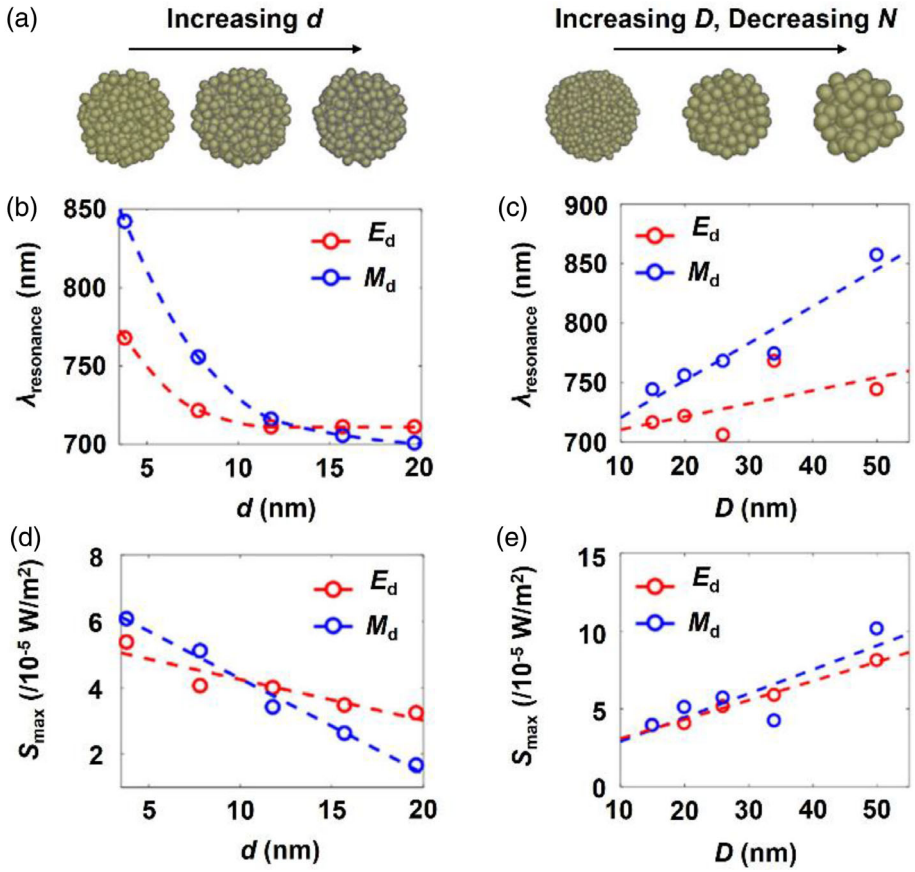


FIGURE 6 (a) Series of simulated models of raspberry-MMs with different interparticle distances (d) and diameters (D). (b, c) Dependence of electric dipole (E_d) and magnetic dipole (M_d) resonance wavelength ($\lambda_{resonance}$) on d (b) and D (c). (d, e) Dependence of E_d and M_d maximum dipolar resonant scattering strength (S_{max}) on d (d) and D (e). Reproduced with permission.[51] Copyright 2018, American Chemical Society.

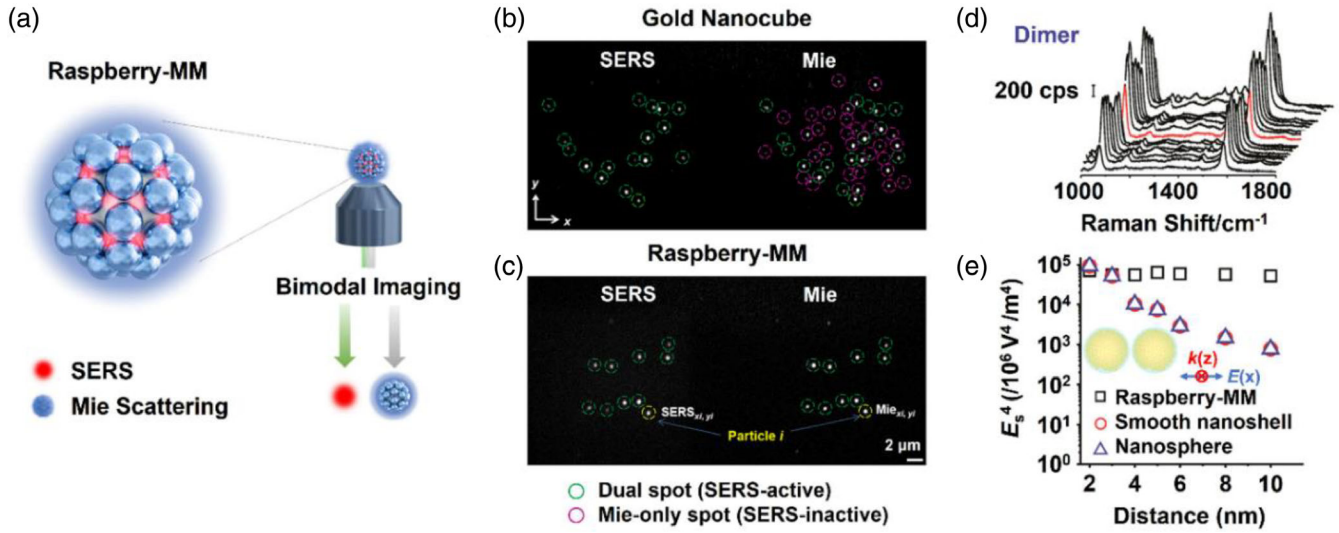


FIGURE 7 Visualization of SERS and Mie scattering signals from raspberry-MMs. (a) Schematic illustration of SERS and Mie scattering signals from a single raspberry-MM. The scheme illustrates the spatial origins of SERS and Mie scattering from a raspberry-MM. The red spots indicate the intraparticle gaps generating SERS signals, whereas the blue highlight represents the Mie resonance. (b, c) Bimodal imaging of SERS and Mie scattering signals from gold nanocube clusters (b) and raspberry-MMs (c). (d) Single-particle SERS data from raspberry-MM dimers with different interparticle distances. (e) Calculated Raman enhancement (E_s^4) of raspberry-MM, smooth nanoshell, and gold nanosphere dimers as a function of the separation distance. (a–c) Reproduced with permission.[52] Copyright 2021, American Chemical Society. (d, e) Reproduced with permission.[50] Copyright 2016, American Chemical Society.

12255949, 2024, 6, Downloaded from https://onlinelibrary.wiley.com/doi/10.1002/bkcs.12845 by Ewha Womans University Library, Wiley Online Library on [16/01/2025]. See the Terms and Conditions (https://onlinelibrary.wiley.com/terms-and-conditions) on Wiley Online Library for rules of use; OA articles are governed by the applicable Creative Commons License

spaced nanoparticle assembly structure. Detailed studies on structure-property relationships provided us with important lessons on materials design. First, computational and experimental studies showed that the nanoshells with many built-in hot spots exhibit strong SERS signals that are insensitive to the distance between nanoshells. This unique property is highly advantageous for SERS-based sensing. Secondly, the assembled structures are not perfect and possess heterogeneities in the size and shape of metal nanoparticles. In general, such nonuniformity has been considered a negative characteristic. However, computational and experimental studies of the core–shell-type structures discussed here revealed that some degree of heterogeneity can lead to signal enhancement and improved uniformity in SERS. These results provide important guidelines for designing SERS substrates with highly enhanced and more reproducible signals.

Nonetheless, the ability to form uniform assemblies can improve our understanding of the collective properties of metal nanoparticles. We have addressed this issue by incorporating a thermoresponsive polymer core for the self-assembly of nanoparticles.[41,64,65] This new approach enables on-demand dynamic structural control using pre-synthesized uniform nanoparticles, which can lead to in-depth understanding of their complex metamaterial properties. We believe that such dynamic self-assembly will open up exciting opportunities for both fundamental investigations and new applications.

ACKNOWLEDGMENTS

This study was supported by National Research Foundation of Korea grants, funded by the Government of Korea (MSIT) (NRF-2017R1A5A1015365, RS-2023-00274736).

ORCID

Sunghee Lee https://orcid.org/0000-0002-4984-308X
So-Jung Park https://orcid.org/0000-0002-6364-3754

REFERENCES

[1] Y. Xia, N. J. Halas, *MRS Bull.* **2005**, *30*, 338.
[2] S. Eustis, M. A. El-Sayed, *Chem. Soc. Rev.* **2006**, *35*, 209.
[3] K. A. Willets, R. P. Van Duyne, *Annu. Rev. Phys. Chem.* **2007**, *58*, 267.
[4] K. L. Kelly, E. Coronado, L. L. Zhao, G. C. Schatz, *J. Phys. Chem. B* **2003**, *3*, 668.
[5] P. K. Jain, K. S. Lee, I. H. El-Sayed, M. A. El-Sayed, *J. Phys. Chem. B* **2006**, *110*, 7238.
[6] K.-S. Lee, M. A. El-Sayed, *J. Phys. Chem. B* **2006**, *110*, 19220.
[7] P. K. Jain, M. A. El-Sayed, *Chem. Phys. Lett.* **2010**, *487*, 153.
[8] N. J. Halas, S. Lal, W.-S. Chang, S. Link, P. Nordlander, *Chem. Rev.* **2011**, *111*, 3913.
[9] C. Sönnichsen, B. M. Reinhard, J. Liphardt, A. P. Alivisatos, *Nat. Biotechnol.* **2005**, *23*, 741.
[10] B. M. Reinhard, M. Siu, H. Agarwal, A. P. Alivisatos, J. Liphardt, *Nano Lett.* **2005**, *5*, 2246.
[11] P. K. Jain, S. Eustis, M. A. El-Sayed, *J. Phys. Chem. B* **2006**, *110*, 18243.
[12] S. J. Oldenburg, S. L. Westcott, R. D. Averitt, N. J. Halas, *J. Chem. Phys.* **1999**, *111*, 4729.
[13] K.-H. Su, Q.-H. Wei, X. Zhang, J. Mock, D. R. Smith, S. Schultz, *Nano Lett.* **2003**, *3*, 1087.
[14] C. Tabor, R. Murali, M. Mahmoud, M. A. El-Sayed, *J. Phys. Chem. A* **2009**, *113*, 1946.
[15] C. Zhou, X. Duan, N. Liu, *Acc. Chem. Res.* **2017**, *50*, 2906.
[16] F. Neubrech, M. Hentschel, N. Liu, *Adv. Mater.* **2020**, *32*, 1905640.
[17] A. Alù, A. Salandrino, N. Engheta, *Opt. Express* **2006**, *14*, 1557.
[18] A. Alu, N. Engheta, *Opt. Express* **2009**, *17*, 5723.
[19] F. Monticone, A. Alu, *J. Mater. Chem. C* **2014**, *2*, 9059.
[20] J. H. Huh, K. Kim, E. Im, J. Lee, Y. Cho, S. Lee, *Adv. Mater.* **2020**, *32*, 2001806.
[21] S. Lee, K. Sim, S. Y. Moon, J. Choi, Y. Jeon, J. M. Nam, S. J. Park, *Adv. Mater.* **2021**, *33*, 2007668.
[22] Z. Li, Q. Fan, Y. Yin, *Chem. Rev.* **2021**, *122*, 4976.
[23] J. M. Kim, C. Lee, Y. Lee, J. Lee, S. J. Park, S. Park, J. M. Nam, *Adv. Mater.* **2021**, *33*, 2006966.
[24] A. Acharya, I. S. Lee, *Bull. Korean Chem. Soc.* **2022**, *43*, 1342.
[25] C. M. Soukoulis, S. Linden, M. Wegener, *Science* **2007**, *315*, 47.
[26] N. Liu, H. Guo, L. Fu, S. Kaiser, H. Schweizer, H. Giessen, *Nat. Mater.* **2008**, *7*, 31.
[27] N. Liu, S. Mukherjee, K. Bao, L. V. Brown, J. Dorfmüller, P. Nordlander, N. J. Halas, *Nano Lett.* **2012**, *12*, 364.
[28] N. J. Greybush, I. Liberal, L. Malassis, J. M. Kikkawa, N. Engheta, C. B. Murray, C. R. Kagan, *ACS Nano* **2017**, *11*, 2917.
[29] C. Matricardi, C. Hanske, J. L. Garcia-Pomar, J. Langer, A. Mihi, L. M. Liz-Marzan, *ACS Nano* **2018**, *12*, 8531.
[30] N. J. Greybush, V. Pacheco-Peña, N. Engheta, C. B. Murray, C. R. Kagan, *ACS Nano* **2019**, *13*, 1617.
[31] S. Mühlig, A. Cunningham, S. Scheeler, C. Pacholski, T. Bürgi, C. Rockstuhl, F. Lederer, *ACS Nano* **2011**, *5*, 6586.
[32] S. Mühlig, C. Rockstuhl, V. Yannopapas, T. Bürgi, N. Shalkevich, F. Lederer, *Opt. Express* **2011**, *19*, 9607.
[33] J. Dintinger, S. Mühlig, C. Rockstuhl, T. Scharf, *Opt. Mater. Express* **2012**, *2*, 269.
[34] S. N. Sheikholeslami, H. Alaeian, A. L. Koh, J. A. Dionne, *Nano Lett.* **2013**, *13*, 4137.
[35] Z. Qian, S. P. Hastings, C. Li, B. Edward, C. K. McGinn, N. Engheta, Z. Fakhraai, S.-J. Park, *ACS Nano* **2015**, *9*, 1263.
[36] R. P. Höller, M. Dulle, S. Thomä, M. Mayer, A. M. Steiner, S. Förster, A. Fery, C. Kuttner, M. Chanana, *ACS Nano* **2016**, *10*, 5740.
[37] S. Gomez-Graña, A. Le Beulze, M. Treguer-Delapierre, S. Mornet, E. Duguet, E. Grana, E. Cloutet, G. Hadziioannou, J. Leng, J. B. Salmon, V. G. Kravets, A. N. Grigorenko, N. A. Peyyety, V. Ponsinet, P. Richetti, A. Baron, D. Torrent, P. Barois, *Mater. Horiz.* **2016**, *3*, 596.
[38] A. Le Beulze, S. Gomez-Graña, H. Gehan, S. Mornet, S. Ravaine, M. Correa-Duarte, L. Guerrini, R. A. Alvarez-Puebla, E. Duguet, E. Pertreux, A. Crut, P. Maioli, F. Vallée, N. Del Fatti, O. Ersen, M. Treguer-Delapierre, *Nanoscale* **2017**, *9*, 5725.
[39] U. Manna, J.-H. Lee, T.-S. Deng, J. Parker, N. Shepherd, Y. Weizmann, N. F. Scherer, *Nano Lett.* **2017**, *17*, 7196.
[40] M. R. Bourgeois, A. T. Liu, M. B. Ross, J. M. Berlin, G. C. Schatz, *J. Phys. Chem. C* **2017**, *121*, 15915.
[41] S. Lee, C. N. Woods, O. Ibrahim, S. W. Kim, S. B. Pyun, E. C. Cho, Z. Fakhraai, S.-J. Park, *J. Phys. Chem. C* **2020**, *124*, 20436.
[42] S. Lim, J. E. Song, J. A. La, E. C. Cho, *Chem. Mater.* **2014**, *26*, 3272.
[43] Z. Qian, K. N. Guye, D. J. Masiello, D. S. Ginger, *J. Phys. Chem. B* **2017**, *121*, 1092.
[44] J. H. Yoon, J. Lim, S. Yoon, *ACS Nano* **2012**, *6*, 7199.
[45] G. A. Vinnacombe-Willson, Y. Conti, A. Stefancu, P. S. Weiss, E. Cortés, L. Scarabelli, *Chem. Rev.* **2023**, *123*, 8488.
[46] B. L. Sanchez-Gaytan, S.-J. Park, *Langmuir* **2010**, *26*, 19170.
[47] B. L. Sanchez-Gaytan, P. Swanglap, T. J. Lamkin, R. J. Hickey, Z. Fakhraai, S. Link, S.-J. Park, *J. Phys. Chem. C* **2012**, *116*, 10318.
[48] B. L. Sanchez-Gaytan, Z. Qian, S. P. Hastings, M. L. Reca, Z. Fakhraai, S.-J. Park, *J. Phys. Chem. C* **2013**, *117*, 8916.
[49] S. P. Hastings, P. Swanglap, Z. Qian, Y. Fang, S.-J. Park, S. Link, N. Engheta, Z. Fakhraai, *ACS Nano* **2014**, *8*, 9025.
[50] Z. Qian, C. Li, Z. Fakhraai, S.-J. Park, *J. Phys. Chem. C* **2016**, *120*, 1824.
[51] C. Li, S. Lee, Z. Qian, C. Woods, S.-J. Park, Z. Fakhraai, *J. Phys. Chem. C* **2018**, *122*, 6808.

12295949, 2024, 6, Downloaded from https://onlinelibrary.wiley.com/doi/10.1002/bkcs.12845 by Ewha Womans University Library, Wiley Online Library on [16/01/2025]. See the Terms and Conditions (https://onlinelibrary.wiley.com/terms-and-conditions) on Wiley Online Library for rules of use; OA articles are governed by the applicable Creative Commons License

[52] S. Lee, J. Kim, K. Baek, N. H. Kim, J. K. Hyun, S.-J. Park, H. Lee, *J. Phys. Chem. Lett.* **2021**, *12*, 5889.
[53] Y. Zheng, Y. Ma, J. Zeng, X. Zhong, M. Jin, Z. Y. Li, Y. Xia, *Chemistry—Asian J.* **2013**, *8*, 792.
[54] Y. Zheng, X. Zhong, Z. Li, Y. Xia, *Part. Part. Syst. Charact.* **2014**, *31*, 266.
[55] Z. Wang, R. Gao, B. Nikoobakht, M. El-Sayed, *J. Phys. Chem. B* **2000**, *104*, 5417.
[56] N. Garg, C. Scholl, A. Mohanty, R. Jin, *Langmuir* **2010**, *26*, 10271.
[57] M. Brown, B. J. Wiley, *Chem. Mater.* **2020**, *32*, 6410.
[58] H. Wang, G. P. Goodrich, F. Tam, C. Oubre, P. Nordlander, N. J. Halas, *J. Phys. Chem. B* **2005**, *109*, 11083.
[59] B. E. Brinson, J. B. Lassiter, C. S. Levin, R. Bardhan, N. Mirin, N. J. Halas, *Langmuir* **2008**, *24*, 14166.
[60] S. Oldenburg, R. Averitt, S. Westcott, N. Halas, *Chem. Phys. Lett.* **1998**, *288*, 243.
[61] W. Shi, Y. Sahoo, M. T. Swihart, P. Prasad, *Langmuir* **2005**, *21*, 1610.
[62] C. Oubre, P. Nordlander, *J. Phys. Chem. B* **2005**, *109*, 10042.
[63] G. Chen, Y. Wang, M. Yang, J. Xu, S. J. Goh, M. Pan, H. Chen, *J. Am. Chem. Soc.* **2010**, *132*, 3644.
[64] O. Ibrahim, S. Lee, S. W. Kim, S. B. Pyun, C. Woods, E. C. Cho, S.-J. Park, Z. Fakhraai, *J. Phys. Chem. C* **2021**, *125*, 16605.
[65] S. Lee, O. Ibrahim, Z. Fakhraai, S.-J. Park, *J. Phys. Chem. C* **2022**, *126*, 6668.

AUTHOR BIOGRAPHIES

Sunghee Lee received her PhD in Chemistry and Nanoscience from Ewha Womans University, under the guidance of Prof. So-Jung Park. Her PhD work was focused on the synthesis, assembly, and properties of plasmonic nanoparticles. She is currently a postdoctoral researcher in the Department of Chemical and Biomolecular Engineering and School of Dental Medicine at the University of Pennsylvania.

Soyun Lee completed her BS in Chemistry and Nanoscience at Ewha Womans University in South Korea. She obtained her MS degree in Chemistry and Nanoscience from Ewha Womans University, under the supervision of Prof. So-Jung Park. Her research was focused on multimetallic nanoparticles.

Soojin Hwang received her BS in Chemistry and Nanoscience from Ewha Womans University in South Korea. She is currently a MS candidate in Chemistry and Nanoscience at Ewha Womans University, under the guidance of Prof. So-Jung Park. Her current research focuses on DNA-directed assembly of metal nanoparticles and their properties.

So-Jung Park received her PhD in Chemistry at Northwestern University in 2002 under the supervision of Prof. Chad Mirkin and conducted her postdoctoral research with Prof. Paul Barbara at University of Texas in Austin. She started her independent career at the Department of Chemistry at the University of Pennsylvania in 2005. In 2013, she moved to Department of Chemistry and Nanoscience at Ewha Womans University, as a full professor. She is serving as an Associate Editor of *ACS Applied Materials and Interfaces* and is on the Advisory Board of *Nanoscale*, *Nanoscale Advances*, and *Bioconjugate Chemistry*. Her current research focuses on plasmonic nanomaterials, dynamic self-assembly, and functional block copolymers.

How to cite this article: S. Lee, S. Lee, S. Hwang, S.-J. Park, *Bull. Korean Chem. Soc.* **2024**, *45*(6), 486. https://doi.org/10.1002/bkcs.12845

12295949, 2024, 6, Downloaded from https://onlinelibrary.wiley.com/doi/10.1002/bkcs.12845 by Ewha Womans University Library, Wiley Online Library on [16/01/2025]. See the Terms and Conditions (https://onlinelibrary.wiley.com/terms-and-conditions) on Wiley Online Library for rules of use; OA articles are governed by the applicable Creative Commons License